Chemical Science

ROYAL SOCIETY OF CHEMISTRY

EDGE ARTICLE

View Article Online
View Journal | View Issue

Cite this: *Chem. Sci.*, 2021, **12**, 14833

All publication charges for this article have been paid for by the Royal Society of Chemistry

Highly efficient carbazolylgold(III) dendrimers based on thermally activated delayed fluorescence and their application in solution-processed organic light-emitting devices†‡

Lok-Kwan Li, Wing-Kei Kwok, Man-Chung Tang, Wai-Lung Cheung, Shiu-Lun Lai, Maggie Ng, Mei-Yee Chan * and Vivian Wing-Wah Yam *

Received 7th July 2021
Accepted 27th September 2021

DOI: 10.1039/d1sc03690d

rsc.li/chemical-science

A new class of C^C^N ligand-containing carbazolylgold(III) dendrimers has been designed and synthesized. High photoluminescence quantum yields of up to 82% in solid-state thin films and large radiative decay rate constants in the order of 10^5 s^{-1} are observed. These gold(III) dendrimers are found to exhibit thermally activated delayed fluorescence (TADF), as supported by variable-temperature emission spectroscopy, time-resolved photoluminescence decay and computational studies. Solution-processed organic light-emitting diodes (OLEDs) based on these gold(III) dendrimers have been fabricated, which exhibit a maximum current efficiency of 52.6 cd A^{-1}, maximum external quantum efficiency of 15.8% and high power efficiency of 41.3 lm W^{-1}. The operational stability of these OLEDs has also been recorded, with the devices based on zero- and second-generation dendrimers showing maximum half-lifetimes of 1305 and 322 h at 100 cd m^{-2}, respectively, representing the first demonstration of operationally stable solution-processed OLEDs based on gold(III) dendrimers.

Introduction

While organic light-emitting devices (OLEDs) have been widely adopted in various electronic devices nowadays, the first commercial product equipped with an OLED display was based on light-emitting polymeric materials.[1] The reduced production cost and material usage are advantageous over vacuum deposition for manufacturing large area displays and lighting systems.[2–4] Apart from traditional fluorescence-based polymers,[5–7] there are increasing efforts on the development of phosphorescent metal-containing polymers[8,9] and thermally activated delayed fluorescent (TADF) polymers,[10–12] mainly arising from their ability to harvest both singlet and triplet excitons for light emission, and a yield of unity for the internal quantum efficiency. However, commonly encountered problems, such as batch-to-batch reproducibility and wide molecular weight distribution associated with polymer chemistry, have remained one of the biggest challenges for commercialization.[2,10]

Dendrimers are considered as a viable class of alternatives due to their well-controlled synthesis; particularly, their modular feature allows them to be functionalized to show specific functions, such as electron-transporting or hole-transporting properties.[13–19] Among them, carbazole dendrimers with TADF properties have been vastly explored for OLED applications, attributed to their high luminescence quantum yields, good film formation abilities and excellent hole-transport properties.[2] Yamamoto and co-workers first reported carbazole dendrimers of up to generation four with a triazine core as TADF materials for solution-processable OLEDs in 2015.[20] The estimated lowest-lying singlet excited state (S_1)–lowest-lying triplet excited state (T_1) energy gap (ΔE_{ST}) values of these dendrimers were found to be as small as 0.03 eV, owing to their completely separated highest occupied molecular orbitals (HOMOs) and lowest unoccupied molecular orbitals (LUMOs). However, strong luminescence quenching was also observed in these dendrimers under aerated conditions,[20] similar to small molecule-based TADF emitters.[21–26] Since then, extensive research on TADF carbazole–anthracene-9,10-dione,[27] carbazole–phosphine oxide,[28] carbazole–sulfone[29] and carbazole–cyanophenyl dendrimers[30–32] has been carried out to improve their luminescence properties. OLEDs based on these dendrimers exhibit extraordinary electroluminescence (EL) performance with a maximum external quantum efficiency (EQE) of

Institute of Molecular Functional Materials, Department of Chemistry, The University of Hong Kong, Pokfulam Road, Hong Kong, P. R. China. E-mail: wwyam@hku.hk; chanmym@hku.hk; Fax: +852-2857-1586; Tel: +852-2859-2153

† Dedicated to Professor Christian Bruneau.

‡ Electronic supplementary information (ESI) available: Thermogravimetric analysis; PL spectra of the gold(III) dendrimers in solid-state thin films; simulated UV-vis spectra of the gold(III) complexes; spatial plots of selected frontier MOs; orbital energy diagrams; plots of the spin density of the emissive states; TDDFT/CPCM orbital and excitation energies; Cartesian coordinates; EL spectra and EQEs of the gold(III) OLEDs. See DOI: 10.1039/d1sc03690d

20.4%.[30] Apart from pure organic compounds, dendritic (alkyl)(amino) carbene metal-containing TADF emitters based on gold(I) and copper(I) metal centers have been reported, in which the solution-processed OLEDs based on these emitters exhibit a maximum EQE of 10.3% at a practical brightness level of 1000 cd m^{-2},[33] demonstrating the high potential of metal-containing TADF dendrimers as emitting materials for OLED applications.

Meanwhile, our research group has been working on luminescent gold(III) dendrimers for OLED applications since our first reports on the small-molecule gold(III) system in 2005 and the dendritic gold(III) system in 2013;[3] particularly, different types of conjugated and saturated dendritic ligands based on triphenylamine,[34] carbazole,[19,35] fluorene–carbazole,[36–39] fluorene–triphenylamine[36,37,39] and poly(aryl)ether dendrons[40] have been incorporated into the gold(III) metal center. With the judicious choice of cyclometalating and dendritic alkynyl ligands, tunable emission colors from sky-blue to near-infrared have been achieved in the C^N^C ligand-containing alkynylgold(III) systems.[34–36] Following our OLED studies on gold(III) systems,[34–36] Che and co-workers very recently reported tridentate and tetradentate ligand-containing gold(III) complexes that demonstrated EL performance and operational stability in vacuum-deposited OLEDs.[41–43] These small-molecular based gold(III) complexes were found to exhibit TADF properties, as supported by their fast radiative decay rate constant (k_r) in the order 10^5 s^{-1}, completely separated frontier orbitals, variable temperature emission and excited-state decay studies. It is worth noting that a large k_r value of $\sim 1.36 \times 10^5$ s^{-1} could also be found in our recently reported alkynylgold(III) dendrimers,[39] indicating that the emission is not purely originating from the triplet excited state.[41–43]

Recent reports have demonstrated that the photophysical properties of cyclometalated gold(III) complexes can be significantly enriched upon replacing the more common C^N^C type of ligand framework with the C^C^N moiety,[44–46] owing to the suppressed non-radiative decay rate constant *via* the distorted triplet state. Taking advantage of the rich photoluminescence behavior found in the solid state, herein we report the synthesis of first- and second-generation carbazolylgold(III) dendrimers (**2** and **3**), which are higher generation dendrimers of a previously reported structurally related small-molecule carbazolylgold(III) complex, [Au{4-^{t}BuC^C(4-^{t}BuC$_6$H$_4$)^N$_{(py)}$}(Cbz)] (**1**).[45] Scheme 1 illustrates the molecular structures of **1–3**. These dendrimers show high photoluminescence quantum yields (PLQYs) of up to 82% and emission lifetimes of less than 3 μs in solid-state thin films, with k_r in the order 10^5 s^{-1}. Interestingly, the luminescence intensities of these dendrimers are found to be enhanced by up to 5-fold upon increasing the temperature from 77 to 300 K, typical of the

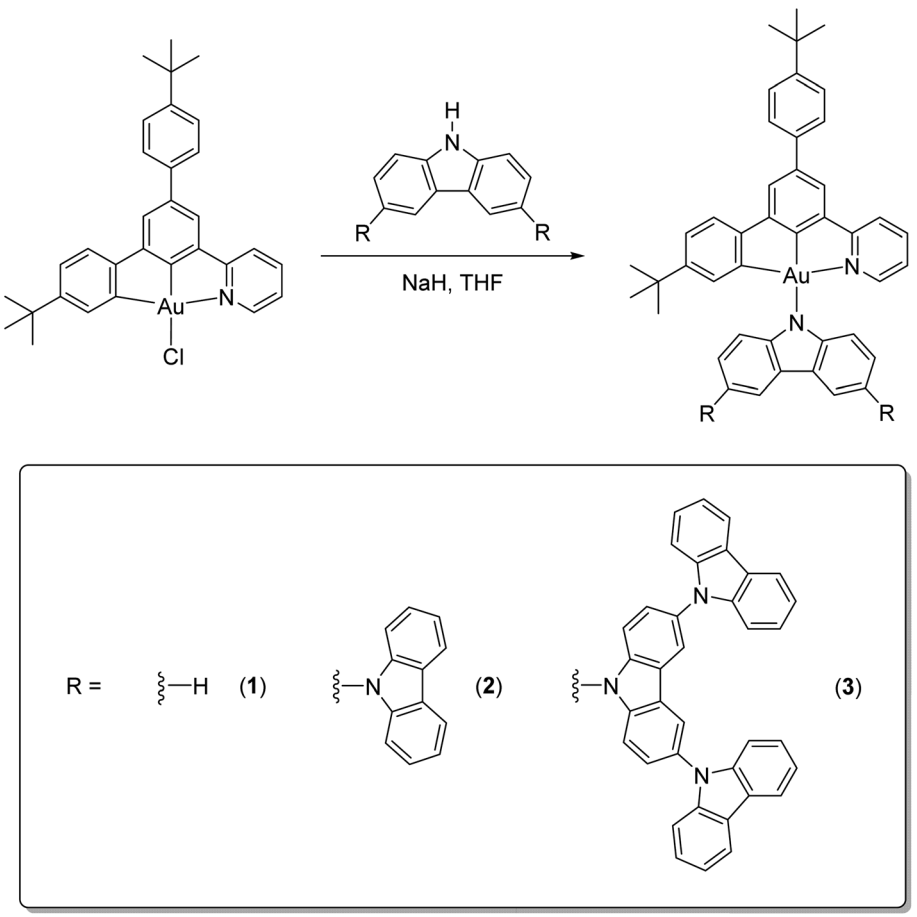

Scheme 1 Synthetic route for the tridentate C^C^N ligand-containing carbazolylgold(III) dendrimers **1–3**.

emission behavior of TADF emitters. Variable-temperature emission studies have been conducted to estimate the ΔE_{ST} of the representative complex **1**, which is found to be *ca.* 0.003 eV. Such a small ΔE_{ST} value of these dendrimers is also supported by time-dependent density functional theory (TDDFT) calculations, suggesting facile intersystem crossing (ISC) and reverse intersystem crossing (RISC) processes and hence efficient TADF properties in these dendrimers. High performance solution-processed OLEDs have been realized based on these dendrimers; notably, devices based on the second-generation dendrimer show a maximum current efficiency (CE) of 41.3 cd A^{-1} and EQE of 15.8%. More importantly, the operational stability of the solution-processed OLEDs has been recorded, in which the devices based on **1** and **3** exhibit maximum operational half-lifetimes of 1305 and 322 h at 100 cd m^{-2}, respectively, representing the first demonstration of operationally stable solution-processed OLEDs based on gold(III) dendrimers.

Results and discussion

Synthesis, characterization and thermal stability

The carbazole dendrimers were synthesized by a palladium-catalyzed Buchwald–Hartwig cross-coupling reaction according to the literature,[33] while **1–3** were synthesized by reacting the chlorogold(III) precursor, [Au{4-^{t}BuC^C(4-^{t}BuC$_6$H$_4$)^N}Cl], with sodium hydride and the corresponding carbazole dendrimers of different generations in degassed tetrahydrofuran (Scheme 1).[45] All the complexes have been well-characterized by ^{1}H and ^{13}C{^{1}H} nuclear magnetic resonance (NMR) spectroscopy and isolated as thermally stable solids. The decomposition temperatures (T_d) are found to significantly increase from **1** (347 °C) to **2** (387 °C) to **3** (459 °C) (Fig. S1 and Table S1‡). These results demonstrate that the incorporation of more carbazole units onto the ancillary ligand could lead to higher robustness, thus rendering higher thermal stability in the higher generation dendrimers.

Electrochemistry

The electrochemical properties of **1–3** in dichloromethane (0.1 M ^{n}Bu$_4$NPF$_6$) at 298 K have been examined, with their cyclic voltammograms showing the oxidative and reductive scans depicted in Fig. 1 and the data listed in Table 1. In general, all the dendrimers exhibit an irreversible reduction wave at −1.69 V to −1.77 V *vs.* the saturated calomel electrode (SCE), attributed to the ligand-centered reduction of the C^C^N ligand. On the other hand, their oxidation behaviors are different from each other. While **1** exhibits an irreversible oxidation wave at +0.86 V *vs.* SCE, **2** and **3** show quasi-reversible first oxidation waves with anodic peak potentials (E_{pa}) at +0.87 V and +0.95 V *vs.* SCE, respectively, corresponding to first oxidation couples ($E^{ox}_{1/2}$) at +0.83 V and +0.91 V *vs.* SCE. These oxidation wave and couples are attributed to the ligand-centered oxidation of the carbazole ligand.[45] Additionally, the higher generation gold(III) dendrimers **2** and **3** show a second oxidation wave at +1.34 V and +1.39 V *vs.* SCE, respectively, which are assigned to the oxidation of the peripheral carbazole units of the dendrimers. The observed oxidation behaviour is found to be in good agreement with the luminescence and computational studies

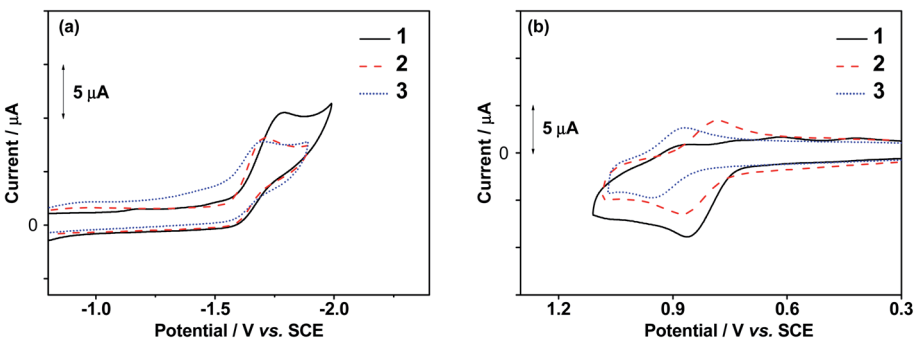

Fig. 1 Cyclic voltammograms showing the (a) reductive and (b) oxidative scans of **1–3** in dichloromethane (0.1 M ^{n}Bu$_4$NPF$_6$).

Table 1 Electrochemical data of **1–3**[a]

Complex	Oxidation $E^{ox}_{1/2}$/V *vs.* SCE[b] [E_{pa}/V *vs.* SCE][c] (ΔE_p/mV)[d]	Reduction [E_{pc}/V *vs.* SCE][e]	E_{HOMO}[f]/eV	E_{LUMO}[g]/eV
1	[+0.86]	[−1.77]	−5.20	−2.57
2	+0.83 (78), [+1.34]	[−1.70]	−5.17	−2.64
3	+0.91 (72), [+1.39]	[−1.69]	−5.21	−2.65

[a] In CH_2Cl_2 solution with 0.1 M ^{n}Bu$_4$NPF$_6$ as the supporting electrolyte at 298 K; working electrode, glassy carbon; scan rate = 100 mV s^{-1}. [b] $E^{ox}_{1/2} = (E_{pa} + E_{pc})/2$; E_{pa} and E_{pc} are the peak anodic and peak cathodic potentials, respectively. [c] E_{pa} refers to the anodic peak potential for the irreversible oxidation waves. [d] $\Delta E_p = (E_{pa} - E_{pc})$. [e] E_{pc} refers to the cathodic peak potential for the irreversible reduction waves. [f] E_{HOMO} levels were calculated from electrode potentials, *i.e.* $E_{HOMO} = -[E_{pa}$ (*vs.* Fc^+/Fc) + 4.80] eV or $E_{HOMO} = -[E^{ox}_{1/2}$ (*vs.* Fc^+/Fc) + 4.80] eV. $E°(Fc^+/Fc)$ = +0.46 V *vs.* SCE in CH_2Cl_2 (0.1 M ^{n}Bu$_4$NPF$_6$). From ref. 47. [g] E_{LUMO} levels were calculated from electrode potentials, *i.e.* $E_{LUMO} = -[E_{pc}$ (*vs.* Fc^+/Fc) + 4.80] eV. $E°(Fc^+/Fc) = +0.46$ V *vs.* SCE in CH_2Cl_2 (0.1 M ^{n}Bu$_4$NPF$_6$). From ref. 47.

(see below), in which the increase in the number of carbazole units in the ancillary ligand from **1** to **2** results in the destabilization of the π orbital of the carbazole ligand due to an extended π-conjugation, and a further increase in the number of carbazole units from **2** to **3** leads to the stabilization of the π orbital of the carbazole ligand as a result of the negative inductive effect exerted by the peripheral carbazole units.

Photophysical properties

The UV-vis absorption and emission spectra of **1–3** in toluene at 298 K are shown in Fig. 2a and b, respectively, while the photophysical data are summarized in Table 2. All complexes exhibit intense absorption bands at wavelength (λ) ≤ 380 nm, with the extinction coefficient (ε) in the order of 10^4 to 10^5 dm^3 mol^{-1} cm^{-1}, and an absorption tail extending to *ca.* 400–500 nm. Similar to the observation found for the previously reported gold(III) dendrimers,[35] the molar extinction coefficient of the absorption band at *ca.* 290–330 nm for these complexes is found to increase with increasing dendrimer generations; such a high-energy absorption band for all the complexes is therefore assigned as the spin-allowed intraligand (IL) [π → π*(carbazole)] transition.[35] On the other hand, the absorption bands at *ca.* 335–380 nm are attributed to the IL [π → π*(C^C^N)] transition, with some phenyl-to-pyridine charge transfer character, while the absorption tail is assigned to the ligand-to-ligand charge transfer (LLCT) [π(carbazole) → π*(C^C^N)] transition.[48–51] The absorption edge is found to be red-shifted from **1** to **2**, which can be explained by the increased conjugation length in the first-generation dendrimer.[14] However, as the dendrimer generation further increases from **2** to **3**, a blue shift in the absorption edge is observed. It is proposed that the steric hindrance experienced by the peripheral carbazole moieties has led to a highly twisted conformation in the second-generation dendrimer, such that the negative inductive effect becomes more prominent than the resonance effect.[14] Upon excitation at $\lambda \geq 350$ nm in degassed toluene, **1–3** exhibit structureless emission bands with peak maxima at *ca.* 584–624 nm. These emission bands are assigned as originating from the LLCT [π(carbazole) → π*(C^C^N)] excited state.[48–51] Interestingly, a slight red shift of the emission band is observed going from **1** (607 nm) to the first-generation dendrimer **2** (624 nm). These results may suggest that the effect of extending π-conjugation of the carbazole ligand and the negative inductive effect exerted by the nitrogen atoms of the peripheral carbazole moieties are acting opposite to each other, resulting in a slight destabilization of the π orbital of carbazole ligand in **2** when compared to **1**. Further increase in the number of carbazole units in the dendrons makes the electron-withdrawing effect more dominating, leading to a hypsochromic shift of the emission peak maximum of the second-generation dendrimer **3** (*i.e.* 584 nm).[35] These results are found to be in good agreement with the electrochemical and computational studies (see below).

A similar trend of the emission behavior is observed in the thin films of 10 wt% **1–3** doped into 1,3-bis(carbazol-9-yl) benzene (mCP). As shown in Fig. 2c, **1** and **2** exhibit structureless emission bands peaking at 536 nm,[48–51] while **3** shows a high-energy shoulder at 503 nm, in addition to a structureless low-energy emission band peaking at 525 nm. The emission bands are assigned as originating from a mixture of higher-lying IL [π → π*(C^C^N)] and lower-lying LLCT [π(carbazole) → π*(C^C^N)] excited states. Upon increasing the dopant concentration, bathochromic shifts of the emission energies have been observed and are commonly ascribed to excimeric emission arising from the π–π stacking of the cyclometalating ligand.[48–51] However, the extent of the red shift has been found to be less significant in the present dendrimers, as shown in Fig. S2–S4,‡ when compared with our previous studies.[35] In this regard, we propose that the red shifts of the emission energies are attributed to the change in the molecular packing in the solid state and the polarity of the host-matrix environment,[52] given that the ground-state dipole moments (μ) of mCP, gold(III) dendrimers **1**, **2** and **3** are 1.32 D, 9.05 D, 13.08 D and 18.39 D, respectively, as supported by the computational studies. Remarkably, the emission shoulder of **3** is found to disappear upon increasing the dopant concentration from 20 to 100 wt% along with reduced excited state lifetimes, in which these emission bands can be well-fitted to the single exponential decay model. Time-resolved emission studies have also been performed on the solid-state thin films of **3**. As shown in

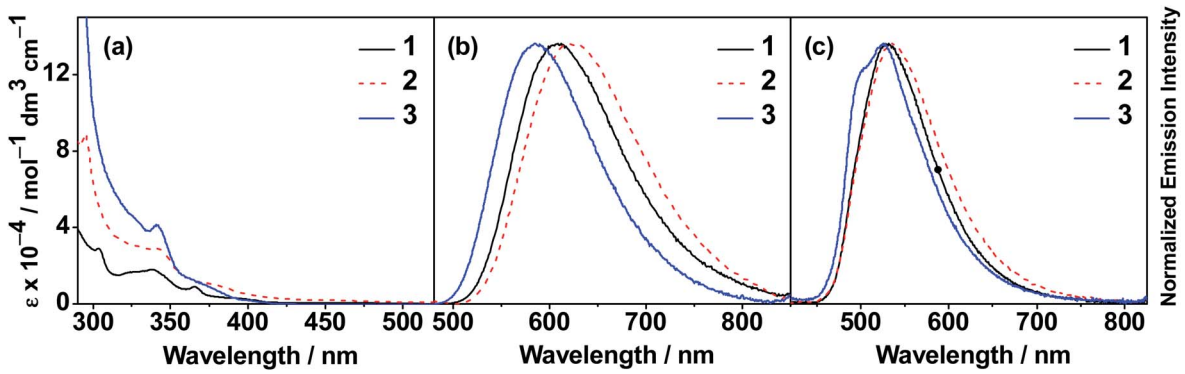

Fig. 2 (a) UV-vis absorption and (b) normalized emission spectra of **1–3** in toluene at 298 K. (c) Normalized emission spectra of thin films of 10 wt% **1–3** doped into mCP at 298 K.

Table 2 Photophysical data of **1–3**

Complex	Medium (T/K)	Absorption λ_{max}/nm (ε_{max}/dm^3 mol^{-1} cm^{-1})	Emission λ_{max}/nm (τ_o/μs)	Φ_{sol}[a]	Φ_{film}[b]	k_r[c]/s^{-1}	k_{nr}[c]/s^{-1}
1	Toluene (298)	326 (16 490), 338 (17 720), 365 (8920), 485 (310)	607 (0.5)	0.040		8.0×10^4	1.9×10^6
	Solid (298)		514 (1.9)				
	Solid (77)		523 (3.7, 8.6)[f]				
	Glass (77)[d]		520, 555 (24.8)				
	Thin film (298)[e]						
	5 wt% in mCP		529 (8.1)		0.73	9.0×10^4	3.3×10^4
	10 wt% in mCP		536 (5.8)		0.75	1.2×10^5	5.2×10^4
	15 wt% in mCP		545 (4.1)		0.79	1.9×10^5	5.1×10^4
	20 wt% in mCP		547 (3.5)		0.74	2.1×10^5	7.4×10^4
					0.82[g]	2.3×10^5	5.1×10^4
2	Toluene (298)	295 (89 355), 341 (29 320), 380 (9800)	624 (0.2)	0.036		1.8×10^5	4.8×10^6
	Solid (298)		568 (0.2)				
	Solid (77)		545, 581 (0.7, 3.6)[f]				
	Glass (77)[d]		482, 518, 555 (3.1, 21.6)[f]				
	Thin film (298)[e]						
	5 wt% in mCP		532 (1.4)		0.74	5.3×10^5	1.9×10^5
	10 wt% in mCP		536 (1.3)		0.64	4.9×10^5	2.8×10^5
	15 wt% in mCP		540 (1.2)		0.61	5.1×10^5	3.3×10^5
	20 wt% in mCP		543 (1.1)		0.59	5.4×10^5	3.7×10^5
					0.68[g]	6.2×10^5	2.9×10^5
	50 wt% in mCP		560 (1.1)		0.48	4.4×10^5	4.7×10^5
3	Toluene (298)	294 (176 210), 341 (41 395), 373 (9730)	584 (0.5)	0.091		1.8×10^5	1.8×10^6
	Solid (298)		565 (0.4)				
	Solid (77)		557 (2.4)				
	Glass (77)[d]		491, 533, 569 (2.8, 15.7)[f]				
	Thin film (298)[e]						
	5 wt% in mCP		503, 525 (0.7, 3.1)		0.58	1.9×10^5	1.4×10^5
	10 wt% in mCP		503, 525 (0.4, 2.4)		0.54	2.3×10^5	1.9×10^5
	15 wt% in mCP		525 (1.6)		0.55	3.4×10^5	2.8×10^5
	20 wt% in mCP		525 (1.6)		0.58	3.6×10^5	2.6×10^5
					0.75[g]	4.7×10^5	1.6×10^5
	50 wt% in mCP		535 (1.4)		0.37	2.6×10^5	4.5×10^5
	75 wt% in mCP		552 (0.9)		0.28	3.1×10^5	8.0×10^5
	100 wt% in mCP		567 (0.5)		0.11	2.2×10^5	1.8×10^6

[a] The relative luminescence quantum yields were measured at room temperature using quinine sulfate in 0.5 M H_2SO_4 as the reference (excitation wavelength = 365 nm, $\Phi_{lum} = 0.546$). [b] Φ_{film} of gold(III) compound doped into mCP excited at a wavelength of 310 nm. [c] Radiative decay rate constant determined from the equation $k_r = \Phi_{em}/\tau$; non-radiative decay rate constant determined from the equation $k_{nr} = (1 - \Phi_{em})/\tau$. [d] Measured in EtOH–MeOH–CH_2Cl_2 (40 : 10 : 1, v/v). [e] Prepared by spin-coating. [f] Bi-exponential decay. [g] Measured under inert atmosphere.

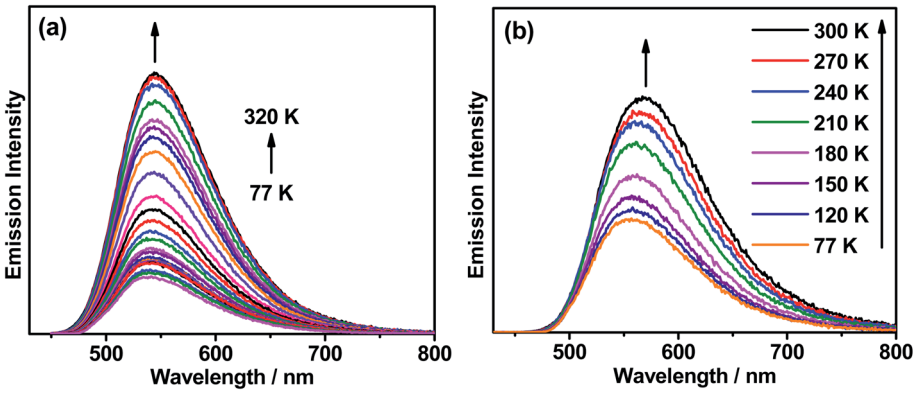

Fig. 3 (a) Emission spectra of the thin film of 20 wt% **1** doped in mCP upon increasing the temperature from 77 to 320 K. (b) Emission spectra of the neat film of **3** upon increasing the temperature from 77 to 300 K.

Fig. S5,‡ the emission band of **3** in the 20 wt% doped thin film gradually changed from Gaussian-shaped to vibronic-structured as the delay time was increased from 0 ns to 15 μs. This may be attributed to the involvement of ^{3}IL and LLCT excited states in the emission. On the other hand, both emission band shapes and energies in the neat film of **3** are independent of the delay time; particularly, a clean Gaussian-shaped emission band typical of LLCT emission is observed. These findings indicate that the LLCT excited state, which usually shows a Gaussian-shaped emission band, has been stabilized to a greater extent relative to the ^{3}IL excited state, which usually shows vibronic-structured emission.[53,54] Such stabilization of the LLCT state would remove the possible complication of an involvement of a spin-allowed reverse internal conversion between the close-lying ^{3}IL and LLCT excited states (TSDP process), allowing further investigation on the TADF properties observed in the LLCT excited state of these dendrimers.[41,55]

Thermally enhanced luminescence

To elucidate the TADF properties of this series of gold(III) dendrimers, temperature-dependent emission studies have been conducted on **1** and **3** in solid-state thin films, with their emission spectra at various temperatures shown in Fig. 3. Upon increasing the temperature from 77 to 300 K, the intensity of the structureless emission band is found to gradually increase, regardless of the faster non-radiative decay rate at higher temperatures. A similar phenomenon has also been observed in other TADF compounds, which have been reported to display an increase in the PLQY of the delayed emission at higher temperatures.[21] As shown in Fig. 3a, the intensity of the emission band of **1** is found to drastically increase by 5 fold with increasing temperature from 77 to 320 K, which is due to the increased rate constant of RISC (k_{RISC}) as well as the reducing involvement of the weakly emissive ^{3}IL state at higher temperatures. However, the emission intensity gradually decreases upon further increasing the temperature from 320 to 360 K (Fig. S6‡). This indicates a faster non-radiative process when compared to the thermally enhanced luminescence above 320 K. Similar enhancement in the intensity of the emission band of **3** is observed as the temperature increases from 77 to 300 K (Fig. 3b). Variable-temperature studies on the excited-state lifetime of **1** in solid-state thin film have been conducted as the representative example. It is worth noting that the excited state lifetimes of **1** are almost unchanged in the range of 200 K (1.3 μs) to 320 K (1.2 μs), suggesting that the thermal up-conversion process is almost complete under these temperature conditions.[56] As the ISC rate constants (k_{ISC}) of structurally related cyclometalated gold(III) complexes are found to be in the picosecond regime,[41–43] much faster than that of the rate constant for fluorescence decay (k_{fl}), the ΔE_{ST} of these complexes can be estimated by fitting the variable-temperature emission data to the full kinetic model employed by Dias, Penfold, and Monkman.[57] Fig. 4 depicts the plot of $\ln(k_{TADF})$ *vs.* $1/T$ of **1**, with a linear slope of $\Delta E_{ST}/k_B$ and an intercept of $[\ln(b)]$, where $[\ln(b)]$ is a function of k_{ISC} and k_{fl} (eqn (1)) and k_B is the Boltzmann constant.[58] It is worth noting that this class of gold(III) dendrimers exhibits emissions with heavily mixed excited states involving ^{3}IL, ^{1}LLCT and ^{3}LLCT, with these excited states being very close-lying in energy. On the other hand, the contribution from ^{3}IL emission is negligible in the temperature range of 200–300 K, as reflected by the k_r values

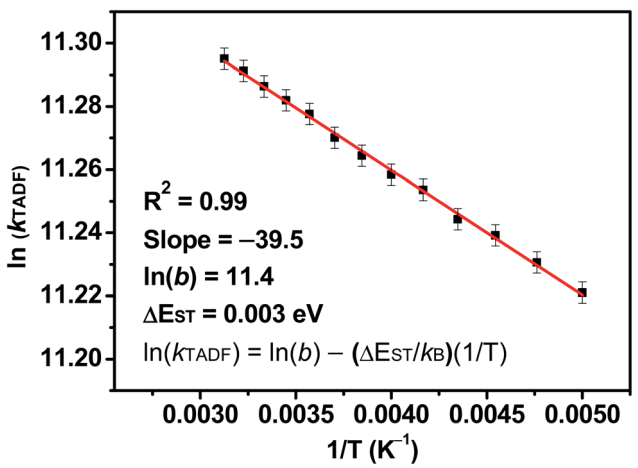

Fig. 4 A plot of $\ln(k_{TADF})$ against $1/T$ in the temperature range of 200 to 320 K and its linear fit to eqn (1) for 20 wt% **1** doped in mCP according to the full kinetic model.

obtained from the variable-temperature emission lifetime measurements that show the same order of magnitude within this temperature range. Thus, it is reasonable to assume that k_r is equivalent to k_{TADF} at this instance. Notably, a small ΔE_{ST} value of 0.003 eV is estimated, which is in line with our calculated value of 0.005 eV (see below). Although this full kinetic model is not the best approach for the calculation of ΔE_{ST} in metal-containing compounds that involve multiple excited states for emission, the good agreement of the ΔE_{ST} value obtained from the model to that obtained from computational studies further confirms the reliability of the method and establishes this class of carbazolylgold(III) dendrimers as TADF active.

$$\ln(k_{TADF}) = \ln\left(\frac{k_{ISC}^{S_1}}{3}\left(1 - \frac{k_{ISC}^{S_1}}{k_{fl} + k_{ISC}^{S_1}}\right)\right) - \frac{\Delta E_{ST}}{k_B T}$$
$$= \ln(b) - \frac{\Delta E_{ST}}{k_B T} \quad (1)$$

Computational studies

To gain a deeper insight into the electronic structures and the nature of the absorption and emission origins of these tridentate-ligand containing gold(III) dendrimers, density functional theory (DFT) and TDDFT calculations have been performed on **2** and **3**. The computational results of **1** reported in our previous studies are also extracted for comparison.[45] The optimized ground-state geometries in both front and side views and the selected structural parameters of **1–3** are shown in Fig. S7.‡ In general, **1–3** show insignificant differences in the bond lengths and bond angles in the cyclometalating ligand. It is observed that there is a small increase in the dihedral angle for N(1)–Au–N(2)–C(3) from **1** to **3** (*i.e.* **1**: 68.2°; **2**: 69.8°; **3**: 71.8°), probably due to the addition of more carbazolyl units in the dendrons, leading to a slightly larger steric repulsion with the C^C^N moiety. The first thirtieth singlet excited states of **1–3**, computed by the TDDFT/conductor-like continuum model (CPCM) method, are summarized in Table S2,‡ and the simulated UV-vis spectra, generated by Multiwfn,[59] are shown in Fig. S8–S10.‡ The relative energies of the optimized T_1 states and their Cartesian coordinates of the optimized S_1 and T_1 geometries are also shown in Tables S3–S13.‡ Selected molecular orbitals involved in the transitions are shown in Fig. S11–S13.‡ The $S_0 \rightarrow S_1$ transitions computed at *ca.* 480–520 nm are mainly contributed by the HOMO → LUMO excitation. The HOMOs of **1–3** are the π orbitals predominantly localized on the carbazole moieties, while the LUMOs are the π* orbitals predominantly localized on the central phenyl ring and the pyridyl moieties of the C^C^N ligand. Therefore, the HOMO → LUMO transition can be assigned as the LLCT [π(carbazole) → π*(C^C^N)] transition, supporting the experimental energy trend of the absorption bands and their spectral assignments. Consistent with the trend in the UV-vis absorption spectra, the lowest-energy absorption band in **1** is computed at 520 nm, which is significantly lower in energy than those in **2** (502 nm) and **3** (477 nm). The intense absorption bands computed at *ca.* 380 nm correspond to the HOMO−2 → LUMO excitation in **1**, the HOMO−6 → LUMO excitation in **2**, and the HOMO−10 → LUMO excitation in **3**, where the HOMO−2 in **1**, HOMO−6 in **2** and HOMO−10 in **3** are predominantly the π orbital on the phenyl rings of the C^C^N ligand. These absorption bands can be assigned as the IL [π → π*(C^C^N)] transitions with some charge transfer character from the phenyl rings to the pyridyl moieties, which are in line with the experimental assignment.

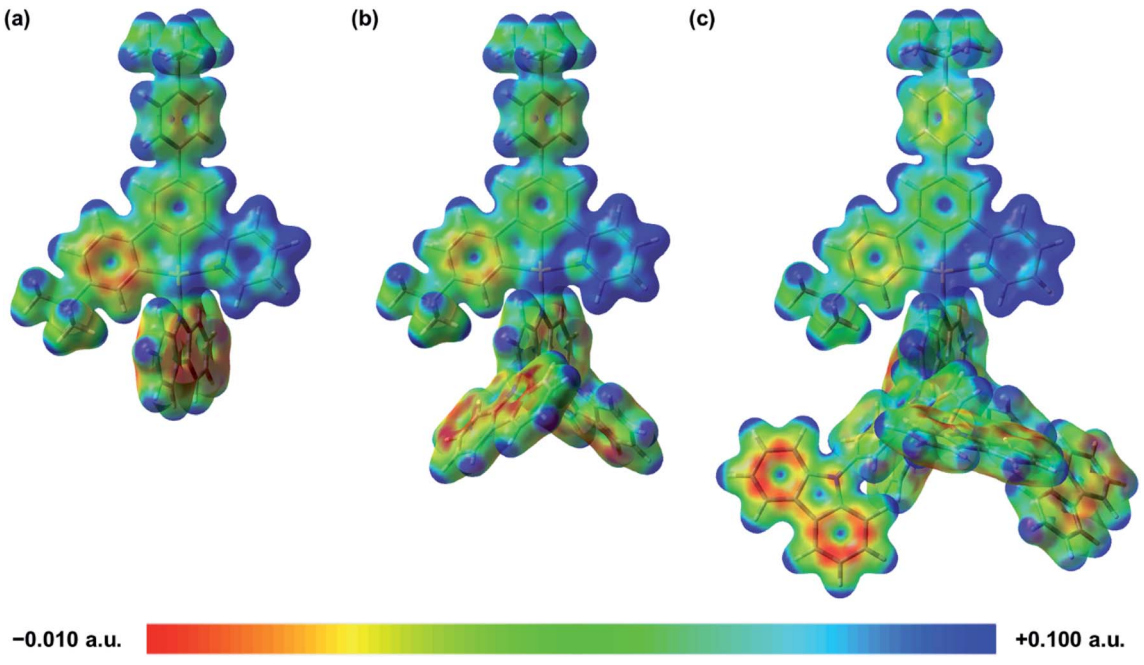

Fig. 5 Calculated electrostatic potential surfaces (isovalue = 0.02) of (a) **1**, (b) **2** and (c) **3**.

Table 3 Computed energy difference between the S_1 and T_1 states (ΔE_{ST}), rate constants of fluorescence (k_{fl}) and phosphorescence (k_{ph}), the average radiative decay rate constant ($k_{r,avg}$), reorganization energy (λ), and the rate constants of the ISC (k_{ISC}) and RISC (k_{RISC}) processes. The energies are in eV and the rate constants are in s^{-1}

Complex	ΔE_{ST}	k_{fl}	k_{ph}	$k_{r,avg}$	λ	k_{ISC}	k_{RISC}
1	6.1×10^{-3}	2.0×10^{5}	5.9×10^{1}	4.3×10^{4}	8.4×10^{-4}	4.4×10^{9}	3.5×10^{9}

The orbital energy diagram showing the frontier molecular orbitals of **1–3** is depicted in Fig. S14.‡ In general, the HOMO energy decreases on going from **1** (−5.11 eV) to **2** (−5.20 eV) to **3** (−5.35 eV), due to the stabilization of the HOMO by the electron-withdrawing carbazolyl units upon increasing the dendron generation. Similarly, the LUMO energy decreases on going from **1** (−2.05 eV) to **2** (−2.17 eV) to **3** (−2.26 eV), owing to the stabilization of the π* orbital of the C^C^N ligand. To gain more insights into the effect of increasing carbazolyl units on the electron densities of the cyclometalating ligand, the electrostatic potential surfaces of the optimized ground-state geometries of **1–3**, shown in Fig. 5, have also been analyzed. Apparently, the incorporation of higher generation of carbazolyl dendrons leads to a more electron-deficient pyridyl moiety, owing to the electron-withdrawing effect of the dendritic carbazolyl substituents, which lowers the electron density on the ancillary carbazolyl N-donor ligand, reducing its electron-donating power. The poorer donor strength of the carbazolyl N-donor ligand would render the metal center more electron-deficient, drawing more electron density from the C^C^N pincer ligand through the σ effect. The less electron-rich metal center would also stabilize the metal dπ orbitals, which in turn would cause a smaller destabilization of the π* (C^C^N) orbital, leading to a lower-lying π* orbital of the C^C^N ligand on going from **1** to **3**. Overall, the HOMO–LUMO energy gap for **2** (3.04 eV) is very slightly narrower than that for **1** (3.06 eV) and **3** (3.09 eV), in good agreement with the experimental trend.

To gain a deeper insight into the nature of the emissive states, the geometries of T_1 of **1–3** have been optimized with the unrestricted UPBE0 method. Their plots of spin density are shown in Fig. S15.‡ In general, the spin density of **1–3** is predominantly localized on the carbazolyl moiety, the central phenyl ring and the pyridyl moiety of the C^C^N ligand, which supports the LLCT [π(carbazole) → π*(C^C^N)] character in the emissive state. The emission wavelengths of **1–3**, approximated by the energy difference between the S_0 and T_1 states at their corresponding optimized geometries are summarized in Table S3.‡ The calculated emission wavelength shows a red shift on going from **3** (507 nm) to **1** (530 nm) to **2** (534 nm) and this is in line with the experimental trend observed in the emission spectra. To gain further insights into the excited states involved in the TADF processes, the geometries of S_1 and T_1 of **1–3** have also been optimized using TDDFT with the Tamm–Dancoff approximation (TDA).[60] The computed ΔE_{ST} values of **1–3** are 0.005, 0.006 and 0.004 eV, respectively. To gain further insight into the kinetics of the ISC and RISC processes of **1**, the ΔE_{ST} value, the rate constants of fluorescence (k_{fl}) and phosphorescence (k_{ph}), the average radiative decay rate constant ($k_{r,avg}$), reorganization energy (λ), and k_{ISC} and k_{RISC} processes have been computed at the PBE0/TZP level using the Amsterdam Density Functional (ADF) program,[61–63] and these thermodynamic and kinetic parameters are summarized in Table 3. ΔE_{ST} computed at the PBE0/TZP level has a value of 0.006 eV, which is in good agreement with the experimental value of 0.003 eV. The computed $k_{r,avg}$ value of 4.3×10^4 s^{-1} is also in agreement with the experimentally determined k_r of 8.0×10^4 s^{-1}, in the same order of magnitude. The computed k_{ISC} and k_{RISC} have high values of 4.4×10^9 and 3.5×10^9 s^{-1}, respectively, in line with the large spin–orbit coupling constant associated with the heavy gold atom, and are found to be comparable, resulting in efficient ISC and RISC processes that facilitate the TADF emission in **1**.

OLED fabrication and characterization

Solution-processed OLEDs based on **1–3** have been prepared to examine their EL properties and operational lifetimes. Fig. 6a

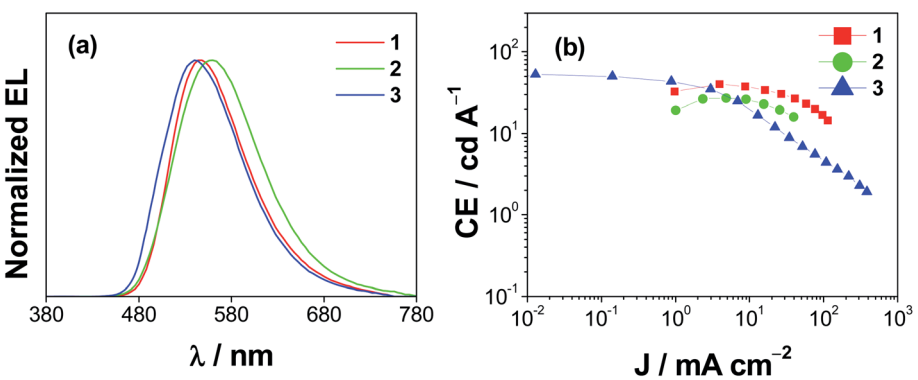

Fig. 6 (a) Normalized EL spectra and (b) CE against current densities of the solution-processed devices based on **1–3**.

depicts the normalized EL spectra of the devices, in which all devices show Gaussian emission with the same trend observed in the emission and computational studies. Particularly, the EL peak maximum is found to be red-shifted on going from **3** (540 nm) to **1** (548 nm) to **2** (560 nm). In addition, smaller bathochromic shifts are found for all the present dendrimers upon increasing the dopant concentrations (see Fig. S16‡). Notably, the EL maximum only slightly red-shifts by *ca.* 8 nm (corresponding to ~278 cm^{-1}) as the concentration of **3** increases from 5 to 20 wt%. These observations are different from those of our previously reported gold(III) dendrimers, in which the emission maximum shifts towards blue with increasing the generation of dendrimers and is strongly dependent on the dopant concentration. A close examination of the absence of a high-energy shoulder in the EL spectra of devices made with **3** further suggests that there is less mixing of excited states between ^{3}IL and ^{3}LLCT, in good agreement with the emission studies.

These TADF properties may boost up the current efficiencies and EQEs of the solution-processed devices. Fig. 6b depicts the current efficiencies (CE) of solution-processed devices made with **1–3** and Table S14‡ summarizes their key characteristics. As we previously reported, devices based on **1** show a maximum CE of 40.0 cd A^{-1} and a maximum EQE of 11.9% at an optimal concentration of 20 wt%.[45] Unexpectedly, the incorporation of carbazole moieties to yield the first-generation dendrimers could not improve the device performance. The maximum CE and EQE of the optimized device made with **2** show a drop to 27.1 cd A^{-1} and 8.7%, respectively. It may be attributed to its poorer solubility in chloroform. On the other hand, further introduction of bulky carbazole units in the periphery of the ancillary ligand significantly increases the dendrimer solubility. Apparently, devices based on 20 wt% **3** demonstrate the highest CE of 52.6 cd A^{-1} and EQE of 15.8%. More importantly, the power efficiency (PE) can be dramatically improved to 41.3 lm W^{-1}. Such a high PE value is comparable to those of the state-of-the-art TADF-based solution-processed devices, as shown in Table S15.‡

Apart from these superior performances, satisfactory operational stabilities can be realized for devices based on these gold(III) dendrimers. Solution-processed devices made with **1** and **3** have been prepared to measure their operational lifetimes at constant driving current densities of 5 and 20 mA cm^{-2}, respectively. A lower driving current density is used for devices based on **1** because of the need for a high driving voltage to reach 20 mA cm^{-2} that exceeded the limit of our equipment. As depicted in Fig. S17 and Table S16,‡ half-lifetimes of devices made with **1** and **3** are 1305 and 322 h, respectively. Although the half-lifetimes are comparatively shorter than those of the vacuum-deposited devices,[45] the present work represents the first demonstration of operationally stable solution-processed OLEDs based on gold(III) dendrimers.

Conclusion

In conclusion, a new class of C^C^N ligand-containing carbazolylgold(III) dendrimers has been designed and synthesized. Temperature-dependent studies show the occurrence of TADF in the gold(III) complexes. These dendrimers are found to exhibit high PLQYs of up to 82% in solid-state thin films. Their TADF properties have been examined by variable-temperature emission, time-resolved photoluminescence decay and computational studies, with estimated ΔE_{ST} values of *ca.* 0.004 eV. The EL properties of solution-processed OLEDs based on these dendrimers have been examined, in which a maximum CE of up to 41.3 cd A^{-1}, EQE of 15.8% and PE of 41.3 lm W^{-1} have been achieved for the device based on the second-generation dendrimer. More importantly, satisfactory operational lifetimes have been recorded, with the devices based on generation zero and two dendrimers exhibiting operational half-lifetimes of up to 1305 and 322 h at 100 cd m^{-2}, respectively, representing the first demonstration of operationally stable solution-processed OLEDs based on gold(III) dendrimers.

Data availability

The datasets supporting this article have been uploaded as part of the ESI material.†

Author contributions

V. W.-W. Y. initiated and designed the research. V. W.-W. Y. and M.-C. T. designed the gold(III) complexes. W.-K. K. conducted the synthesis. L.-K. L., W.-K. K. and M.-C. T. conducted the characterization, photophysical and electrochemical measurements of the gold(III) complexes. L.-K. L. and M. N. performed and analyzed the computational calculations. S.-L. L., W.-L. C. and M.-Y. C. carried out the OLED fabrication and characterizations. V. W.-W. Y. supervised the work. All authors discussed the results and contributed to the manuscript.

Conflicts of interest

The authors declare no competing finanical interest.

Acknowledgements

V. W.-W. Y. acknowledges UGC funding administered by the University of Hong Kong (HKU) for supporting the Electrospray Ionization Quadrupole Time-of-Flight Mass Spectrometry Facilities under the Support for Interdisciplinary Research in Chemical Science and the support from the HKU University Research Committee (URC) Strategically Oriented Research Theme on Functional Materials for Molecular Electronics Towards Materials and Energy Applications, the Croucher-CAS Fund Scheme for Joint Laboratories on Molecular Functional Materials for Electronics, Switching and Sensing and the HKU-TCL Joint Laboratory on New Printable OLED Materials and Technology. This work was supported by Hong Kong Quantum AI Lab Ltd under the AIR@InnoHK cluster of the Innovation and Technology Commission (ITC) and the Research Grants Council (RGC) General Research Fund (GRF) (HKU17306219) of the Hong Kong Special Administrative Region, P. R. China. The computations were performed using the HKU ITS research

computing facilities. W.-K. K. and W.-L. C. acknowledge the receipt of postgraduate studentships from HKU. L.-K. L. acknowledges the receipt of a University Postgraduate Fellowship from the University of Hong Kong.

References

1 J. H. Burroughes, D. D. C. Bradley, A. R. Brown, R. N. Marks, K. Mackay, R. H. Friend, P. L. Burns and A. B. Holmes, Light-emitting diodes based on conjugated polymers, *Nature*, 1990, **347**, 539.

2 P. L. Burn, S.-C. Lo and I. D. W. Samuel, The Development of Light-Emitting Dendrimers for Displays, *Adv. Mater.*, 2007, **19**, 1675.

3 M.-C. Tang, A. K.-W. Chan, M.-Y. Chan and V. W.-W. Yam, Platinum and Gold Complexes for OLEDs, *Top. Curr. Chem.*, 2016, **374**, 46.

4 X. Yang, G. Zhou and W.-Y. Wong, Functionalization of phosphorescent emitters and their host materials by main-group elements for phosphorescent organic light-emitting devices, *Chem. Soc. Rev.*, 2015, **44**, 8484.

5 R. H. Friend, R. W. Gymer, J. H. Holmes, R. N. Marks, C. Taliani, D. D. C. Bradley, D. A. Dos Santos, J. L. Brédas, M. Lögdlund and W. R. Salaneck, Electroluminescence in conjugated polymers, *Nature*, 1999, **397**, 121.

6 C. Schmitz, P. Pösch, M. Theiakkat, H.-W. Schmidt, A. Montali, K. Feldman, P. Smith and C. Weder, Polymeric Light-Emitting Diodes Based on Poly(*p*-phenylene ethynylene), Poly(triphenyldiamine), and Spiroquinoxaline, *Adv. Funct. Mater.*, 2001, **11**, 41.

7 R. B. Inadmuddin, I. A. Mohd and M. A. Abdullah, *Polymers for Light-Emitting Devices and Displays*, Scrivener Publishing LLC, 2020.

8 M. T. Nguyen, R. A. Jones and B. J. Holliday, Recent advances in the functional applications of conducting metallopolymers, *Coord. Chem. Rev.*, 2018, **377**, 237.

9 Q. Zhao, S.-J. Liu and W. Huang, Promising Optoelectronic Materials: Polymers Containing Phosphorescent Iridium(III) Complexes, *Macromol. Rapid Commun.*, 2010, **31**, 794.

10 M. Y. Wong, Recent Advances in Polymer Organic Light-Emitting Diodes (PLED) Using Non-conjugated Polymers as the Emitting Layer and Contrasting Them with Conjugated Counterparts, *J. Electron. Mater.*, 2017, **46**, 6246.

11 Y. Liu, C. Li, Z. Ren, S. Yan and M. R. Bryce, All-Organic Thermally Activated Delayed Fluorescence Materials for Organic Light-Emitting Diodes, *Nat. Rev. Mater.*, 2018, **3**, 18020.

12 X. Yin, Y. He, X. Wang, Z. Wu, E. Pang, J. Xu and J. Wang, Recent Advances in Thermally Activated Delayed Fluorescent Polymer – Molecular Designing Strategies, *Front. Chem.*, 2020, **8**, 725.

13 G. Zhou, W.-Y. Wong, B. Yao, Z. Xie and L. Wang, Triphenylamine-Dendronized Pure Red Iridium Phosphors with Superior OLED Efficiency/Color Purity Trade-Offs, *Angew. Chem., Int. Ed.*, 2007, **46**, 1149.

14 K. Albrecht and K. Yamamoto, Dendritic Structure Having a Potential Gradient: New Synthesis and Properties of Carbazole Dendrimers, *J. Am. Chem. Soc.*, 2009, **131**, 2244.

15 Y. J. Cho, S. A. Hong, H. J. Son, W. S. Han, D. W. Cho and S. O. Kang, Efficient light harvesting and energy transfer in a red phosphorescent iridium dendrimer, *Inorg. Chem.*, 2014, **53**, 13136.

16 J. Ding, J. Gao, Y. Cheng, Z. Xie, L. Wang, D. Ma, X. Jing and F. Wang, Highly Efficient Green-Emitting Phosphorescent Iridium Dendrimers Based on Carbazole Dendrons, *Adv. Funct. Mater.*, 2006, **16**, 575.

17 S. Gambino, S.-C. Lo, Z. Liu, P. L. Burn and I. D. W. Samuel, Charge Transport in a Highly Phosphorescent Iridium(III) Complex-Cored Dendrimer with Double Dendrons, *Adv. Funct. Mater.*, 2012, **22**, 157.

18 T. Imaoka, N. Inoue and K. Yamamoto, Electron-transfer through potential gradient based on a dendrimer architecture, *Chem. Commun.*, 2012, **48**, 7235.

19 F. K.-W. Kong, M.-C. Tang, Y.-C. Wong, M.-Y. Chan and V. W.-W. Yam, Design Strategy for High-Performance Dendritic Carbazole-Containing Alkynylplatinum(II) Complexes and Their Application in Solution-Processable Organic Light-Emitting Devices, *J. Am. Chem. Soc.*, 2016, **138**, 6281.

20 K. Albrecht, K. Matsuoka, K. Fujita and K. Yamamoto, Carbazole Dendrimers as Solution-Processable Thermally Activated Delayed-Fluorescence Materials, *Angew. Chem., Int. Ed.*, 2015, **54**, 5677.

21 H. Uoyama, K. Goushi, K. Shizu, H. Nomura and C. Adachi, Highly efficient organic light-emitting diodes from delayed fluorescence, *Nature*, 2012, **492**, 234.

22 T. Matsushima, F. Bencheikh, T. Komino, M. R. Leyden, A. S. D. Sandanayaka, C. Qin and C. Adachi, High performance from extraordinarily thick organic light-emitting diodes, *Nature*, 2019, **572**, 502.

23 Q. Zhang, B. Li, S. Huang, H. Nomura, H. Tanaka and C. Adachi, Efficient blue organic light-emitting diodes employing thermally activated delayed fluorescence, *Nat. Photonics*, 2014, **8**, 326.

24 T. Ohsawa, H. Sasabe, T. Watanabe, K. Nakao, R. Komatsu, Y. Hayashi, Y. Hayasaka and J. Kido, A Series of Imidazo [1,2-*f*]phenanthridine-Based Sky-Blue TADF Emitters Realizing EQE of over 20%, *Adv. Opt. Mater.*, 2019, **7**, 1801282.

25 P. Li, H. Chan, S.-L. Lai, M. Ng, M.-Y. Chan and V. W.-W. Yam, Four-Coordinate Boron Emitters with Tridentate Chelating Ligand for Efficient and Stable Thermally Activated Delayed Fluorescence Organic Light-Emitting Devices, *Angew. Chem., Int. Ed.*, 2019, **58**, 9088.

26 M. J. Leitl, V. A. Krylova, P. I. Djurovich, M. E. Thompson and H. Yersin, Phosphorescence versus thermally activated delayed fluorescence. Controlling singlet-triplet splitting in brightly emitting and sublimable Cu(I) compounds, *J. Am. Chem. Soc.*, 2014, **136**, 16032.

27 K. Sun, Y. Sun, D. Liu, Y. Feng, X. Zhang, Y. Sun and W. Jiang, CBP derivatives dendronized self-host TADF

dendrimer: achieving efficient non-doped near-infrared organic light-emitting diodes, *Dyes Pigm.*, 2017, **147**, 436.

28 J. Wang, J. Peng, W. Yao, C. Jiang, C. Liu, C. Zhang, M. He, R. Liu, X. Xia and C. Yao, Carbazole-dendrite-encapsulated electron acceptor core for constructing thermally activated delayed fluorescence emitters used in nondoped solution-processed organic light-emitting diodes, *Org. Electron.*, 2017, **48**, 262.

29 X. Ban, W. Jiang, K. Sun, B. Lin and Y. Sun, Self-Host Blue Dendrimer Comprised of Thermally Activated Delayed Fluorescence Core and Bipolar Dendrons for Efficient Solution-Processable Nondoped Electroluminescence, *ACS Appl. Mater. Interfaces*, 2017, **9**, 7339.

30 K. Sun, Y. Sun, W. Tian, D. Liu, Y. Feng, Y. Sun and W. Jiang, Thermally activated delayed fluorescence dendrimers with exciplex-forming dendrons for low-voltage-driving and power-efficient solution-processed OLEDs, *J. Mater. Chem. C*, 2018, **6**, 43.

31 X. Ban, A. Zhu, T. Zhang, Z. Tong, W. Jiang and Y. Sun, Highly Efficient All-Solution-Processed Fluorescent Organic Light-Emitting Diodes Based on a Novel Self-Host Thermally Activated Delayed Fluorescence Emitter, *ACS Appl. Mater. Interfaces*, 2017, **9**, 21900.

32 H. Yersin, A. F. Rausch, R. Czerwieniec, T. Hofbeck and T. Fischer, The triplet state of organo-transition metal compounds. Triplet harvesting and singlet harvesting for efficient OLEDs, *Coord. Chem. Rev.*, 2011, **255**, 2622.

33 A. S. Romanov, L. Yang, S. T. E. Jones, D. Di, O. J. Morley, B. H. Drummond, A. P. M. Reponen, M. Linnolahti, D. Credgington and M. Bochmann, Dendritic Carbene Metal Carbazole Complexes as Photoemitters for Fully Solution-Processed OLEDs, *Chem. Mater.*, 2019, **31**, 3613.

34 M.-C. Tang, C. K.-M. Chan, D. P.-K. Tsang, Y.-C. Wong, M. M.-Y. Chan, K. M.-C. Wong and V. W.-W. Yam, Saturated Red-Light-Emitting Gold(III) Triphenylamine Dendrimers for Solution-Processable Organic Light-Emitting Devices, *Chem.–Eur. J.*, 2014, **20**, 15233.

35 M.-C. Tang, D. P.-K. Tsang, M. M.-Y. Chan, K. M.-C. Wong and V. W.-W. Yam, Dendritic Luminescent Gold(III) Complexes for Highly Efficient Solution-Processable Organic Light-Emitting Devices, *Angew. Chem., Int. Ed.*, 2013, **52**, 446.

36 C.-H. Lee, M.-C. Tang, Y.-C. Wong, M.-Y. Chan and V. W.-W. Yam, Sky-Blue-Emitting Dendritic Alkynylgold(III) Complexes for Solution-Processable Organic Light-Emitting Devices, *J. Am. Chem. Soc.*, 2017, **139**, 10539.

37 M.-C. Tang, C.-H. Lee, M. Ng, Y.-C. Wong, M.-Y. Chan and V. W.-W. Yam, Highly Emissive Fused Heterocyclic Alkynylgold(III) Complexes for Multiple Color Emission Spanning from Green to Red for Solution-Processable Organic Light-Emitting Devices, *Angew. Chem., Int. Ed.*, 2018, **57**, 5463.

38 L.-K. Li, M.-C. Tang, W.-L. Cheung, S.-L. Lai, M. Ng, C. K.-M. Chan, M.-Y. Chan and V. W.-W. Yam, Rational Design Strategy for the Realization of Red- to Near-Infrared-Emitting Alkynylgold(III) Complexes and Their Applications in Solution-Processable Organic Light-Emitting Devices, *Chem. Mater.*, 2019, **31**, 6706.

39 M.-C. Tang, L. H.-Y. Lo, W.-L. Cheung, S.-L. Lai, M.-Y. Chan and V. W.-W. Yam, Green-Emitting Dendritic Alkynylgold(III) Complexes with Excellent Film Morphologies for Applications in Solution-Processable Organic Light-Emitting Devices, *Chem. Commun.*, 2019, **55**, 13844.

40 M.-C. Tang, D. P.-K. Tsang, M.-Y. Chan, K. M.-C. Wong and V. W.-W. Yam, A New Class of Gold(III) Complexes with Saturated Poly(benzyl ether) Dendrons for Solution-Processable Bblue-Green-Emitting Organic Light-Emitting Devices, *Mater. Chem. Front.*, 2017, **1**, 2559.

41 W.-P. To, D. Zhou, G. S. M. Tong, G. Cheng, C. Yang and C.-M. Che, Highly Luminescent Pincer Gold(III) Aryl Emitters: Thermally Activated Delayed Fluorescence and Solution-Processed OLEDs, *Angew. Chem., Int. Ed.*, 2017, **56**, 14036.

42 D. Zhou, W.-P. To, Y. Kwak, Y. Cho, G. Cheng, G. S. M. Tong and C.-M. Che, Thermally Stable Donor–Acceptor Type (Alkynyl)Gold(III) TADF Emitters Achieved EQEs and Luminance of up to 23.4% and 70 300 cd m^{-2} in Vacuum-Deposited OLEDs, *Adv. Sci.*, 2019, **6**, 1802297.

43 D. Zhou, W.-P. To, G. S. M. Tong, G. Cheng, L. Du, D. L. Phillips and C.-M. Che, Tetradentate Gold(III) Complexes as Thermally Activated Delayed Fluorescence (TADF) Emitters: Microwave-Assisted Synthesis and High-Performance OLEDs with Long Operational Lifetime, *Angew. Chem., Int. Ed.*, 2020, **59**, 6375.

44 E. S.-H. Lam, W. H. Lam and V. W.-W. Yam, A Study on the Effect of Dianionic Tridentate Ligands on the Radiative and Nonradiative Processes for Gold(III) Alkynyl Systems by a Computational Approach, *Inorg. Chem.*, 2015, **54**, 3624.

45 L.-K. Li, M.-C. Tang, S.-L. Lai, M. Ng, W.-K. Kwok, M.-Y. Chan and V. W.-W. Yam, Strategies Towards Rational Design of Gold(III) Complexes for High-Performance Organic Light-Emitting Devices, *Nat. Photonics*, 2019, **13**, 185.

46 R. Kumar, A. Linden and C. Nevado, Luminescent (N^C^C) Gold(III) Complexes: Stabilized Gold(III) Fluorides, *Angew. Chem., Int. Ed.*, 2015, **54**, 14287.

47 N. G. Connelly and W. E. Geiger, Chemical Redox Agents for Organometallic Chemistry, *Chem. Rev.*, 1996, **96**, 877.

48 K. M.-C. Wong, X. Zhu, L.-L. Hung, N. Zhu, V. W.-W. Yam and H.-S. Kwok, A Novel Class of Phosphorescent Gold(III) Alkynyl-Based Organic Light-Emitting Devices with Tunable Colour, *Chem. Commun.*, 2005, 2906.

49 V. W.-W. Yam, K. M.-C. Wong, L.-L. Hung and N. Zhu, Luminescent Gold(III) Alkynyl Complexes: Synthesis, Structural Characterization, and Luminescence Properties, *Angew. Chem., Int. Ed.*, 2005, **44**, 3107.

50 V. K.-M. Au, K. M.-C. Wong, D. P.-K. Tsang, M.-Y. Chan, N. Zhu and V. W.-W. Yam, High-Efficiency Green Organic Light-Emitting Devices Utilizing Phosphorescent Bis-cyclometalated Alkynylgold(III) Complexes, *J. Am. Chem. Soc.*, 2010, **132**, 14273.

51 M.-C. Tang, M.-Y. Leung, S.-L. Lai, M. Ng, M.-Y. Chan and V. Wing-Wah Yam, Realization of Thermally Stimulated

Delayed Phosphorescence in Arylgold(III) Complexes and Efficient Gold(III) Based Blue-Emitting Organic Light-Emitting Devices, *J. Am. Chem. Soc.*, 2018, **140**, 13115.

52 M.-Y. Leung, M.-C. Tang, W.-L. Cheung, S.-L. Lai, M. Ng, M.-Y. Chan and V. W.-W. Yam, Thermally Stimulated Delayed Phosphorescence (TSDP)-Based Gold(III) Complexes of Tridentate Pyrazine-Containing Pincer Ligand with Wide Emission Color Tunability and Their Application in Organic Light-Emitting Devices, *J. Am. Chem. Soc.*, 2020, **142**, 2448.

53 C.-H. Lee, M.-C. Tang, F. K.-W. Kong, W.-L. Cheung, M. Ng, M.-Y. Chan and V. W.-W. Yam, Isomeric Tetradentate Ligand-Containing Cyclometalated Gold(III) Complexes, *J. Am. Chem. Soc.*, 2020, **142**, 520.

54 M.-Y. Leung, M.-C. Tang, W.-L. Cheung, S.-L. Lai, M. Ng, M.-Y. Chan and V. Wing-Wah Yam, Thermally Stimulated Delayed Phosphorescence (TSDP)-Based Gold(III) Complexes of Tridentate Pyrazine-Containing Pincer Ligand with Wide Emission Color Tunability and Their Application in Organic Light-Emitting Devices, *J. Am. Chem. Soc.*, 2020, **142**, 2448.

55 S. Shi, M. C. Jung, C. Coburn, A. Tadle, M. R. D. Sylvinson, P. I. Djurovich, S. R. Forrest and M. E. Thompson, Highly Efficient Photo- and Electroluminescence from Two-Coordinate Cu(I) Complexes Featuring Nonconventional *N*-Heterocyclic Carbenes, *J. Am. Chem. Soc.*, 2019, **141**, 3576.

56 R. Czerwieniec, M. J. Leitl, H. H. H. Homeier and H. Yersin, Cu(I) Complexes – Thermally Activated Delayed Fluorescence. Photophysical Approach and Material Design, *Coord. Chem. Rev.*, 2016, **325**, 2.

57 F. B. Dias, T. J. Penfold and A. P. Monkman, Photophysics of Thermally Activated Delayed Fluorescence Molecules, *Methods Appl. Fluoresc.*, 2017, **5**, 012001.

58 R. Hamze, S. Shi, S. C. Kapper, D. S. Muthiah Ravinson, L. Estergreen, M.-C. Jung, A. C. Tadle, R. Haiges, P. I. Djurovich, J. L. Peltier, R. Jazzar, G. Bertrand, S. E. Bradforth and M. E. Thompson, "Quick-Silver" from a Systematic Study of Highly Luminescent, Two-Coordinate, d^{10} Coinage Metal Complexes, *J. Am. Chem. Soc.*, 2019, **141**, 8616.

59 T. Lu and F. Chen, Multiwfn: A Multifunctional Wavefunction Analyzer, *J. Comput. Chem.*, 2012, **33**, 580.

60 S. Hirata and M. Head-Gordon, Time-Dependent Density Functional Theory within the Tamm-Dancoff Approximation, *Chem. Phys. Lett.*, 1999, **314**, 291.

61 http://www.scm.com.

62 G. te Velde, F. M. Bickelhaupt, E. J. Baerends, C. F. Guerra, S. J. A. Van Gisbergen, J. G. Snijders and T. Ziegler, Chemistry with ADF, *J. Comput. Chem.*, 2001, **22**, 931.

63 C. F. Guerra, J. G. Snijders, G. te Velde and E. J. Baerends, Towards an Order-N DFT Method, *Theor. Chem. Acc.*, 1998, **99**, 391.